



Short communication

Polypyrrole-coated LiV₃O₈-nanocomposites with good electrochemical performance as anode material for aqueous rechargeable lithium batteries

L.L. Liu^a, X.J. Wang^a, Y.S. Zhu^a, C.L. Hu^a, Y.P. Wu^{a,*}, R. Holze^{b,**}

^a New Energy and Materials Laboratory (NEML), Department of Chemistry & Shanghai Key Laboratory of Molecular Catalysis and Innovative Materials, Fudan University, Shanghai 200433, China

^b Technische Universität Chemnitz, Institut für Chemie, AG Elektrochemie, D-09107 Chemnitz, Germany

HIGHLIGHTS

- A polypyrrole-coated LiV₃O₈-nanocomposite was prepared.
- It is suggested as anode material for aqueous rechargeable lithium batteries.
- Polypyrrole acts as a conducting matrix as well as a volume change buffer agent.
- It holds LiV₃O₈ nanorods inside the particles during the charge/discharge cycles.
- Electrochemical performance of PPy@LiV₃O₈ is significantly enhanced.

ARTICLE INFO

Article history:

Received 6 June 2012

Received in revised form

5 July 2012

Accepted 30 September 2012

Available online 8 October 2012

Keywords:

ARLB (aqueous rechargeable lithium batteries)

Anode material

LiV₃O₈

Polypyrrole

Coating

ABSTRACT

A polypyrrole-coated LiV₃O₈ nanocomposite was prepared as anode material (negative mass) for aqueous rechargeable lithium batteries and characterized by X-ray diffraction, scanning electron microscopy, and electrochemical measurements. Polypyrrole acts as a conducting matrix as well as a coating agent, which held LiV₃O₈ nanorods inside the particles during the charge/discharge cycles. Results show that the electrochemical performance of the PPy@LiV₃O₈ nanocomposite is significantly enhanced showing higher capacity and better rate capability as well as better cycling performance compared to pristine LiV₃O₈.

© 2012 Elsevier B.V. All rights reserved.

1. Introduction

Electric vehicles (EVs) present a rapidly developing trend in the worldwide automotive industry to solve the environmental pollution caused by vehicles with internal combustion engines. Unfortunately, so far only few types of batteries can meet all requirements for EVs [1–4]. In addition, the use of renewable energy depends on new power sources. Thus it is necessary to develop new types of green battery materials and safer, less-expensive rechargeable battery systems.

In the mid 1990s, a new type of rechargeable lithium battery based on aqueous electrolytes was reported [5,6], which can overcome the disadvantages of nonaqueous lithium ion batteries, such as high cost and safety problems [7]. Recently, it was reported that cycling and rate capability of the electrode materials for aqueous rechargeable lithium batteries (ARLBs) have been greatly improved [7–13]. Layered LiV₃O₈ was proposed as an anode material for electrochemical devices based on its promising characteristics such as high specific capacity, good rate capability and long cycling life [7]. Although LiV₃O₈ nanomaterials with high capacity in aqueous electrolyte solutions have been reported [14–19], their electrochemical performance is still not satisfactory because of the capacity fading upon cycling and poor rate capability.

Polypyrrole (PPy) is one of the most popular conducting polymers which has been used to modify electrode materials for lithium

* Corresponding author.

** Corresponding author. Tel. +49 37153131509; fax: +49 37153121269.

E-mail addresses: wuyp@fudan.edu.cn (Y.P. Wu), rudolf.holze@chemie.tu-chemnitz.de (R. Holze).

ion batteries [20–24] where it not only serves as a conducting additive reducing the weight contribution of inert materials in the electrode, but also acts as a coating prohibiting the dissolution of active mass and associated release of metal ions during charge and discharge process. To the best of our knowledge, synthesis and application of PPy-coated LiV₃O₈ composite materials for use in ARLBs has not been reported yet. Here we report the synthesis of a PPy-coated LiV₃O₈ nanocomposite via a low-temperature *in situ* oxidative polymerization route. The structural characterization and electrochemical performance of PPy@LiV₃O₈ nanocomposite are discussed and compared with the pristine LiV₃O₈ material.

2. Experimental

2.1. Preparation of anode materials

All reagents were of analytical grade. Lithium nitrate, ammonium vanadate and citric acid were used as raw materials in the molar ratio 1:3:4. First, lithium nitrate and ammonium vanadate were dissolved in distilled water, then the solution was heated to 80 °C following dropwise addition of a solution of citric acid, which was employed as a chelating agent. After stirring continuously at 80 °C for 6 h, a homogeneous dark blue gel was obtained [25]. The gel was placed in an oven for drying at 120 °C in air for 12 h followed by a heat-treatment at 450 °C for another 5 h in a muffle furnace to get LiV₃O₈.

The PPy@LiV₃O₈ nanocomposite was prepared by chemical polymerization of pyrrole (Py) on the LiV₃O₈ nanorod surface using sodium dodecylbenzenesulfonate (NaDBS) as surfactant and FeCl₃ as oxidant. 0.2 g LiV₃O₈ was dispersed into a flask containing 10 mL aqueous solution of sodium dodecylbenzenesulfonate (0.05 M) and stirred for 0.5 h, then 0.01 g pyrrole (5% wt. of LiV₃O₈) and 10 mL FeCl₃ (0.2 M) solution were injected into the aqueous solution. The mixture was kept at 5 °C for 1 h under stirring. Finally, the obtained composite was filtered, washed with water and ethanol, respectively, and then dried under vacuum at 40 °C overnight.

2.2. Characterization of the prepared anode materials

Crystal structures of the prepared LiV₃O₈ and PPy@LiV₃O₈ nanocomposite were characterized by X-ray powder diffraction (XRD) using a Bruker Analytical X-ray System with CuK_α radiation source filtered by a nickel thin plate. Scanning electron micrographs (SEM) and transmission electron micrographs (TEM) were obtained on a Philips XL30 scanning electron microscope and a JEOL JEM-2010 transmission electron microscope, respectively. Elemental analysis was obtained by Thermo E. IRIS Duo inductively coupled plasma (ICP).

For electrochemical tests, anodes were prepared by pressing a powdered mixture of the sample (PPy@LiV₃O₈ or pristine LiV₃O₈), acetylene black, and poly(tetrafluoroethylene) (PTFE) in a weight ratio of 80:10:10, the obtained sheet was punched into small disks of about 1.5 mg at an apparent area of 0.6 cm². Finally, these disks were pressed onto Ni-grids at a pressure of 1.2 MPa and then dried at 70 °C for 5 h. Galvanostatic charge and discharge (−0.6 to 0.2 V vs. SCE) were performed with a three-electrode electrochemical cell in aqueous 0.5 M Li₂SO₄ solution of pH ≈ 7. A saturated calomel electrode (SCE) and a nickel mesh were used as reference and counter electrodes, respectively. A two-electrode cell consisting of the cathode and the anode with a distance of about 1 cm was used to test the electrochemical properties of PPy@LiV₃O₈/AC and LiV₃O₈/AC, and discharge/charge cut-off voltages were set at 0 and 1.2 V, respectively. Electrochemical impedance spectroscopy (EIS) was carried out with an electrochemical work station (CHI604C, Chenhua Ltd. Co., Shanghai, China). The amplitude of the AC perturbation was 5 mV; the frequency range was 10⁴–10¹ Hz.

Activated carbon (AC) with a specific surface area of about 2800 m² g⁻¹ measured by the BET method and a capacity of about 28.5 mAh g⁻¹ at a current density of 100 mA g⁻¹ was purchased from Ningde Xinseng Chemical Industrial Co., Ltd. and used as received without further treatment.

For electrochemical quartz crystal microbalance experiments, an EQCM (electrochemical quartz crystal microbalance) system was used with 10 MHz AT-cut quartz crystal (Chen Hua, Shanghai) coated with 0.25 cm² gold electrodes. Pristine LiV₃O₈ and PPy@LiV₃O₈ were attached to the gold electrode as a small amount of solid, and they were employed for the microbalance experiments, which were performed in a three-electrode cell using Pt wire as an auxiliary electrode and a saturated calomel electrode (SCE) as a reference. Sauerbrey's equation (Eq. (1)) relates changes of the resonance frequency of a quartz crystal with changes of the electrode mass [26,27]. Experimental values of the C_{EQCM}-coefficient is 1.4 ng Hz⁻¹ for the 10 MHz AT quartz crystal furnished with the 0.25 cm² electrodes. Δm and Δf refer to the electrode mass and the frequency change of the quartz crystal, respectively.

$$\Delta m = -C_{EQCM} \times \Delta f \quad (1)$$

All electrical measurements were performed at ambient temperature. In this context, the term "discharge" means "lithiated" while "charge" means "delithiated".

3. Results and discussion

SEM and TEM micrographs of LiV₃O₈ and PPy@LiV₃O₈ nanocomposite are shown in Fig. 1. Evidently, the as-prepared LiV₃O₈ (Fig. 1a) exists in the shape of nanorods, about 3–4 μm in length and 500 nm in width. In the PPy@LiV₃O₈ nanocomposite (Fig. 1b), it

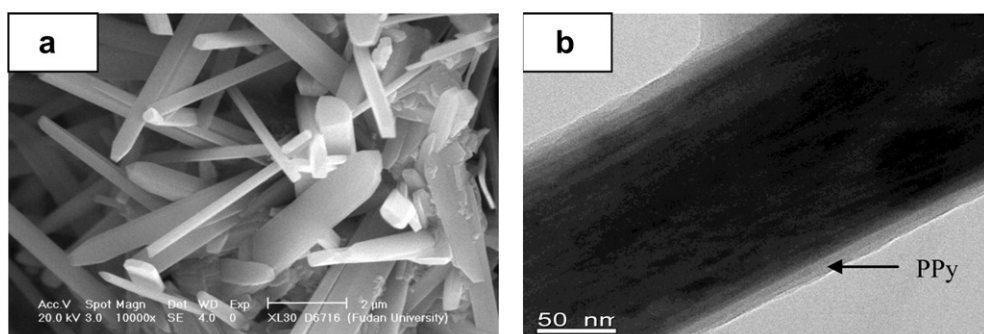


Fig. 1. (a) SEM micrograph of the pristine LiV₃O₈ nanorod and (b) TEM micrograph of the PPy@LiV₃O₈ nanocomposite.

can be clearly seen that the LiV_3O_8 nanorod is uniformly covered with a layer of PPy, and the thickness of the PPy coating is about 14 nm.

XRD patterns of the LiV_3O_8 and PPy@ LiV_3O_8 nanocomposite are shown in Fig. 2. The peak at about $2\theta = 13.9^\circ$ is assigned to the diffraction at (100) planes indicating the layered structure of LiV_3O_8 [16]. The layers consist of VO_6 octahedra and VO_5 square pyramids, which share corners with the octahedra. Li-ions can intercalate between these layers [28,29]. After coating the PPy layer, the crystal structure of LiV_3O_8 in the nanocomposite is still similar to that of LiV_3O_8 except for the peak at about $2\theta = 28^\circ$ indicating the existence of ordered PPy structure [30].

The charge curves at 125 mA cm^{-2} and charge capacities at different current densities of the pristine LiV_3O_8 and the PPy@ LiV_3O_8 nanocomposite between -0.6 and 0.2 V (vs. SCE) in $0.5 \text{ M Li}_2\text{SO}_4$ aqueous electrolyte are shown in Fig. 3. Since the discharge cut-off voltage is -0.6 V vs. SCE, the PPy doping can contribute a little to the reversible capacity and the main reversible capacity for the PPy@ LiV_3O_8 nanocomposite is from the core LiV_3O_8 . It was found that the initial capacity of the PPy@ LiV_3O_8 nanocomposite is higher than that of the pristine LiV_3O_8 . A charge voltage plateau at about -0.2 V vs. SCE for the PPy@ LiV_3O_8 nanocomposite can be more clearly observed compared with the pristine LiV_3O_8 suggesting an enhanced utilization efficiency of LiV_3O_8 material attributable to the improved charge transfer of the nanocomposite [21], as shown in Fig. 3a. The Coulombic efficiency of the composite in the first cycle is higher than that of pristine LiV_3O_8 . The PPy@ LiV_3O_8 nanocomposite exhibits better rate capability than the pristine LiV_3O_8 anode. The specific discharge capacities for the PPy@ LiV_3O_8 nanocomposite are $108, 92$ and 80 mAh g^{-1} at $125, 250$ and 500 mA cm^{-2} , respectively. In contrast, the discharge capacities for the pristine LiV_3O_8 are $75, 63$ and 40 mAh g^{-1} at $125, 250$ and 500 mA cm^{-2} , respectively. The reason for better electrochemical performance of the PPy@ LiV_3O_8 nanocomposite may be the favored intercalation of Li^+ ions into the composite due to the conductive PPy coating [31]. When it is coated on the surface of LiV_3O_8 -nanorods, the electrical conductivity can be significantly increased, which facilitates the charge-transfer reaction, especially at high current densities. As a result, it is easier for the Li^+ to intercalate into the active material, corresponding to a higher capacity and better rate performance.

In order to further explore the function of the PPy, the mass changes of the pristine LiV_3O_8 and the PPy@ LiV_3O_8 nanocomposite electrodes during a cyclic voltammogram in $0.5 \text{ M Li}_2\text{SO}_4$ with a scan rate of 30 mV s^{-1} were measured, as shown in Fig. 4. Obviously, both the pristine LiV_3O_8 and PPy@ LiV_3O_8 nanocomposite

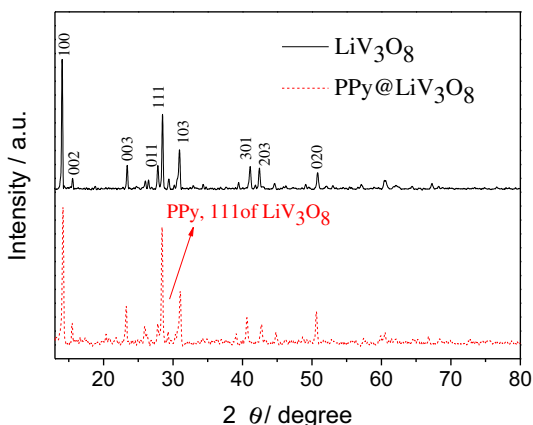


Fig. 2. XRD pattern of the pristine LiV_3O_8 and the PPy@ LiV_3O_8 nanocomposite.

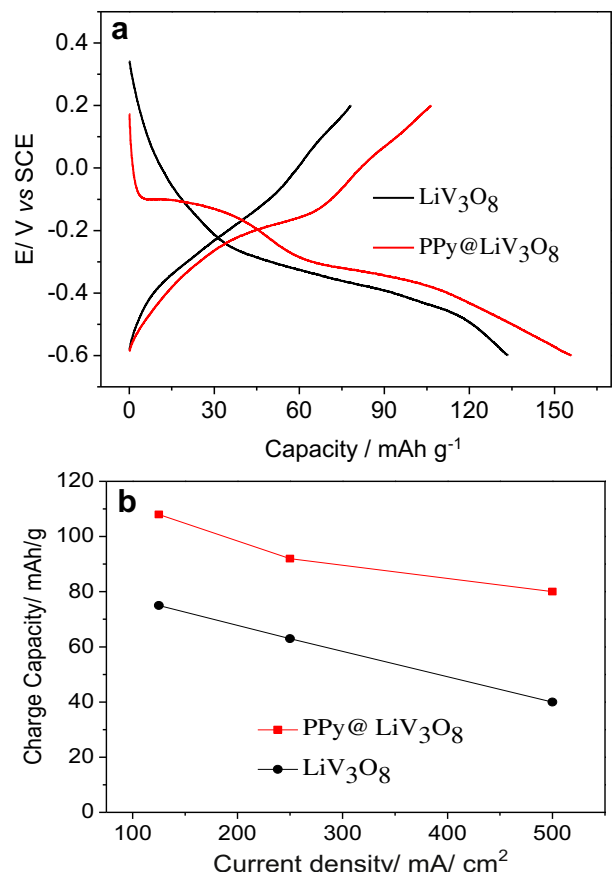


Fig. 3. (a) The charge curves at 125 mA cm^{-2} and (b) the first charge capacities of LiV_3O_8 and the PPy@ LiV_3O_8 nanocomposite in $0.5 \text{ M Li}_2\text{SO}_4$ aqueous electrolyte at various scan rates using SCE as the reference electrode.

present one pair of sharp redox peaks that corresponds to the insertion and extraction of Li^+ ions into and from the LiV_3O_8 layer structure, which also implies that Li^+ can penetrate through the PPy coating and insert into or extract from the LiV_3O_8 . However, the redox peaks of the pristine LiV_3O_8 were located at -0.279 and -0.408 V (vs. SCE) (Fig. 4a) while those of the PPy@ LiV_3O_8 nanocomposite were -0.319 and -0.391 V (vs. SCE) (Fig. 4b). Evidently, ΔE is much smaller for PPy@ LiV_3O_8 . The main reason is that the highly conductive PPy coating decreases the charge transfer resistance of the electrode, thus reducing the polarization [32], which can also explain the better rate performance of the PPy@ LiV_3O_8 nanocomposite.

For pristine LiV_3O_8 (Fig. 4a), a mass gain followed by a mass loss is observed during the reduction process, which is assigned to Li^+ insertion and H_2O extraction. The subsequent oxidation leads to a dramatic mass increase followed by a mass decrease due to the Li^+ extraction and H_2O molecules incorporation into the LiV_3O_8 layers, among which the transportation of H_2O molecules dominates the mass changes, as is shown in Fig. 5a. This result is well supported in the literature [33,34]. From these results we conclude, that the existence of H_2O molecules is not conducive to the Li^+ storage for the LiV_3O_8 .

The EQCM data (Fig. 4b) of the PPy@ LiV_3O_8 nanocomposite reveal that the overall behavior corresponds to mass gain during the reduction and mass loss during the oxidation, so we attribute this to Li^+ insertion during reduction and Li^+ extraction during oxidation considering that the large-size DBS⁻ anions in the PPy matrix are difficult to move. Also, H_2O molecules are not supposed to move through the PPy coating, and it is possible to prevent

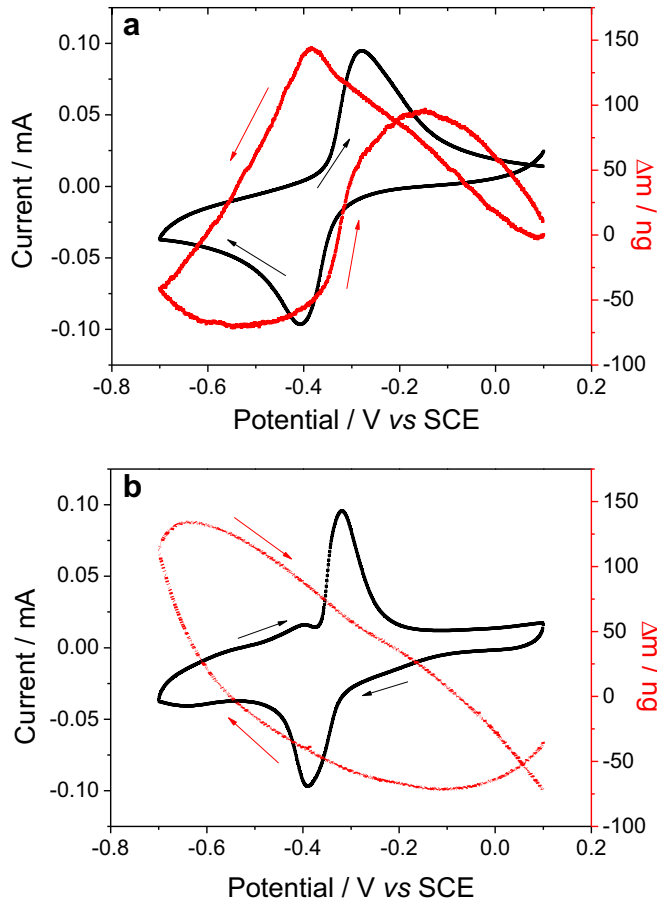


Fig. 4. CVs and mass changes of (a) the pristine LiV_3O_8 and (b) the PPy@ LiV_3O_8 nanocomposite in 0.5 M Li_2SO_4 aqueous electrolyte at a scan rate of 30 mV s^{-1} using SCE as the reference electrode.

structure damages of LiV_3O_8 caused by H_2O molecules. As illustrated in Fig. 5b, PPy coating is expected to facilitate the electronic transport and avoid dissolution of vanadium in the aqueous electrolyte.

Nyquist plots obtained for the pristine LiV_3O_8 and the PPy@ LiV_3O_8 nanocomposite are shown in Fig. 6. Both Nyquist plots consist of two parts, an arc in the high frequency range and an inclining line in the low frequency range. The high frequency range

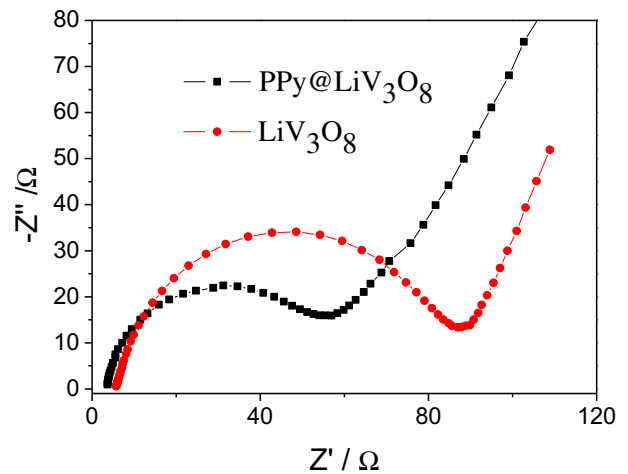


Fig. 6. Nyquist plots of the electrodes from the pristine LiV_3O_8 and the PPy@ LiV_3O_8 nanocomposite.

generally corresponds to the charge transfer resistance and double layer capacitance, and the inclining line in the low frequency range indicates the solid-state diffusion process of lithium ions in LiV_3O_8 [35]. The diameter of the semicircle for the PPy@ LiV_3O_8 nanocomposite is much smaller compared with that of the pristine LiV_3O_8 anode, indicating that the charge transfer resistance of the PPy@ LiV_3O_8 nanocomposite is smaller. Evidently, this is due to the conductive coating of PPy.

The cycling performance of the pristine LiV_3O_8 and the PPy@ LiV_3O_8 nanocomposite using AC as a counter electrode at a rate of 250 mA cm^{-2} between 0 and 1.2 V is shown in Fig. 7. In order to match the capacity, the weight ratio of these two electrodes is fixed at 3.2:1 and 2.2:1 for the pristine LiV_3O_8 and the PPy@ LiV_3O_8 , respectively. Our former results showed that the AC can absorb and desorb alkali ions with good reversibility [36]. It can be observed that the reversible capacity of the pristine LiV_3O_8 faded very quickly, and only 53% of the initial capacity remained after 5 cycles. However, after coating with PPy, the capacity fading of the PPy@ LiV_3O_8 nanocomposite was effectively limited, and 84% of the initial capacity could be obtained after 10 cycles. These results show clearly that the good cycleability of the PPy@ LiV_3O_8 nanocomposite is caused by the PPy coating, which not only increases the conductivity of the nanocomposite favoring lower electron transfer resistance, but also acts as an effective coating that buffers the

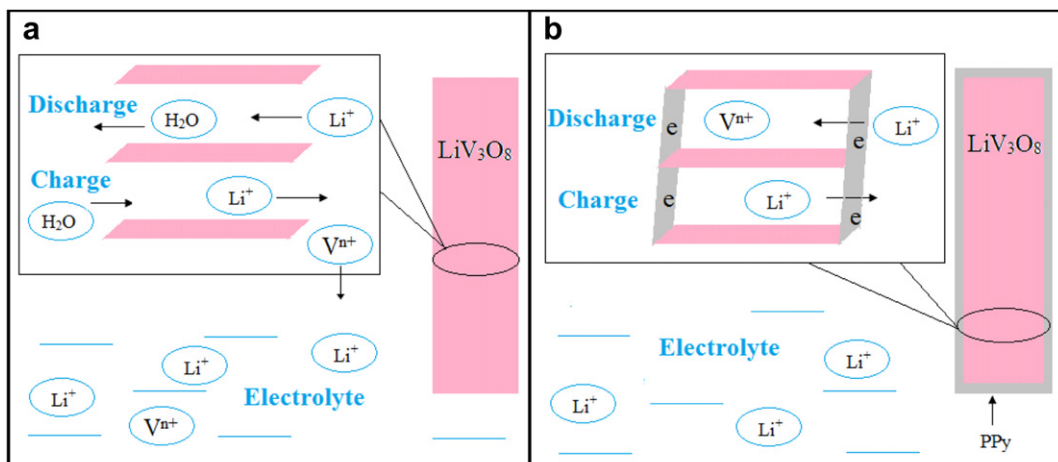


Fig. 5. Schematic illustration of lithium insertion and extraction for (a) the pristine LiV_3O_8 and (b) the PPy@ LiV_3O_8 nanocomposite in aqueous electrolyte.

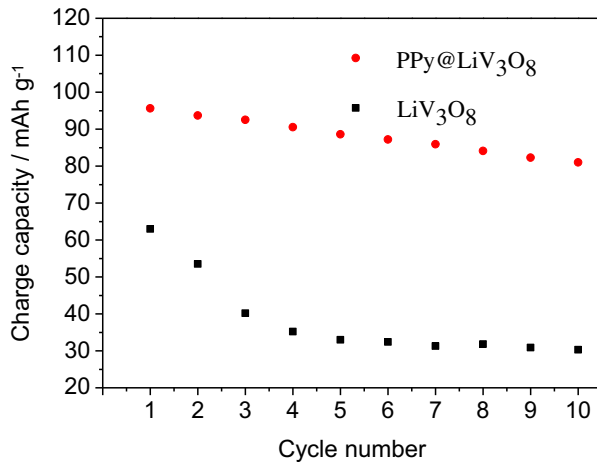


Fig. 7. Cycling performance of the pristine LiV_3O_8 and the $\text{PPy}@\text{LiV}_3\text{O}_8$ nanocomposite using activated carbon (AC) as a counter electrode at a current density of 250 mA cm^{-2} between 0 and 1.2 V.

volume change of LiV_3O_8 during charge/discharge cycles and prevents the dissolution of vanadium thus achieving good structural stability [14]. Elemental analysis results from inductively coupled plasma (ICP) show that the electrolyte after 10 cycles of LiV_3O_8 electrode possess $28.0 \mu\text{g mL}^{-1}$ of vanadium while $2.57 \mu\text{g mL}^{-1}$ for the $\text{PPy}@\text{LiV}_3\text{O}_8$ nanocomposite, which shows that the pristine LiV_3O_8 suffers a more serious dissolution of vanadium than the $\text{PPy}@\text{LiV}_3\text{O}_8$ nanocomposite.

4. Conclusions

A nanocomposite of LiV_3O_8 -nanorod coated with conducting polypyrrole is prepared by a simple *in situ* polymerization route. The as-prepared $\text{PPy}@\text{LiV}_3\text{O}_8$ nanocomposite exhibits higher capacity and better rate capability as well as cycleability compared to the pristine LiV_3O_8 anode, which suggests that PPy works well as a conducting and a coating agent inhibiting the dissolution of vanadium for anode of aqueous rechargeable lithium batteries.

Acknowledgments

Financial support from International Science & Technology Cooperation Program of China (2010DFA61770), NSFC (21073046) and Alexander von Humboldt-Foundation is gratefully appreciated.

References

- [1] A.D. Pasquier, I. Plitz, S. Menocal, G. Amatucci, *J. Power Sources* 115 (2003) 171.
- [2] W.A. Oibrien, R.B. Stickel, G.J. May, *J. Power Sources* 67 (1997) 151.
- [3] Y.P. Wu, C.R. Wan, C.Y. Jiang, *Lithium Ion Secondary Batteries*, Chemical Industry Press, Beijing, 2002.
- [4] M. Brousseau, J.P. Lanchat, G. Rigobert, D. Virey, G. Sarre, *J. Power Sources* 68 (1997) 8.
- [5] W. Li, J.R. Dahn, D.S. Wainwright, *Science* 264 (1994) 1115.
- [6] G. James, *Science* 264 (1994) 1084.
- [7] G.J. Wang, L.J. Fu, N.H. Zhao, L.C. Yang, Y.P. Wu, H.Q. Wu, *Angew. Chem. Int. Ed.* 46 (2007) 295.
- [8] A. Eftekhari, *Electrochim. Acta* 47 (2001) 495.
- [9] R. Ruffo, C. Wessells, R.A. Huggins, Y. Cui, *Electrochim. Commun.* 11 (2009) 247.
- [10] Q.T. Qu, G.J. Wang, L.L. Liu, S. Tian, Y. Shi, Y.P. Wu, *Funct. Mater. Lett.* 3 (2010) 151.
- [11] W. Tang, L.L. Liu, S. Tian, L. Li, Y.B. Yue, Y.P. Wu, S.Y. Guan, K. Zhu, *Electrochim. Commun.* 12 (2010) 1524.
- [12] W. Tang, S. Tian, L.L. Liu, L. Li, H.P. Zhang, Y.B. Yue, Y. Bai, Y.P. Wu, K. Zhu, *Electrochim. Commun.* 13 (2011) 205.
- [13] Q.T. Qu, L.J. Fu, X.Y. Zhan, D. Samuelis, L. Li, W.L. Guo, Z.H. Li, Y.P. Wu, J. Maier, *Energy Environ. Sci.* 4 (2011) 3668.
- [14] G.J. Wang, N.H. Zhao, L.C. Yang, Y.P. Wu, H.Q. Hu, R. Holze, *Electrochim. Acta* 52 (2007) 4911.
- [15] G.J. Wang, H.P. Zhang, L.J. Fu, B. Wang, Y.P. Wu, *Eletrochim. Commun.* 9 (2007) 1873.
- [16] G.J. Wang, L.J. Fu, B. Wang, N.H. Zhao, Y.P. Wu, R. Holze, *J. Appl. Electrochem* 38 (2008) 579.
- [17] C. Cheng, Z.H. Li, X.Y. Zhan, Q.Z. Xiao, G.T. Lei, X.D. Zhou, *Electrochim. Acta* 55 (2010) 4627.
- [18] A. Caballero, J. Morales, O.A. Vargas, *J. Power Sources* 195 (2010) 4318.
- [19] L.L. Liu, W. Tang, S. Tian, Y. Shi, Y.P. Wu, *Funct. Mater. Lett.* 4 (2011) 315.
- [20] Q.T. Qu, Y.S. Zhu, X.W. Gao, Y.P. Wu, *Adv. Energy Mater.* 2 (2012). <http://dx.doi.org/10.1002/aenm.201200088>.
- [21] S. Kuwabata, S. Masui, H. Tomiyori, H. Yoneyama, *Electrochim. Acta* 46 (2000) 91.
- [22] W. Tang, L.L. Liu, S. Tian, Y.S. Zhu, Y.P. Wu, K. Zhu, *Energy Environ. Sci.* 5 (2012) 6909.
- [23] A.J. Heeger, *Angew. Chem. Int. Ed.* 40 (2001) 2591.
- [24] Z. Yin, Q. Zheng, *Adv. Energy Mater.* 2 (2012) 179.
- [25] X.H. Liu, J.Q. Wang, J.Y. Zhang, S.R. Yang, *J. Mater. Sci.* 42 (2007) 867.
- [26] M.R. Deakin, D.A. Buttry, *Anal. Chem.* 61 (1989) 1147A.
- [27] D.A. Buttry, *Electroanal.* 17 (1991) 1.
- [28] G. Pistoia, S. Panero, M. Tocci, R.V. Moshtev, V. Manev, *Solid State Ionics* 13 (1984) 311.
- [29] L.A. dePicciotto, K.T. Adendorff, D.C. Liles, M.M. Thackeray, *Solid State Ionics* 62 (1993) 297.
- [30] K. Huang, M.X. Wan, Y.Z. Long, Z.J. Chen, Y. Wei, *Synth. Met* 155 (2005) 495.
- [31] S.Y. Chew, C.Q. Feng, S.H. Ng, J.Z. Wang, Z.P. Guo, H.K. Liu, *J. Electrochem. Soc.* 154 (2007) A633.
- [32] H.B. Wang, Y.Q. Zeng, K.L. Huang, S.Q. Liu, L.Q. Chen, *Electrochim. Acta* 52 (2007) 5102.
- [33] H. Kanoh, W. Tang, Y. Makita, K. Ooi, *Langmuir* 13 (1997) 6845.
- [34] Q.T. Qu, Y. Shi, L.L. Li, W.L. Guo, Y.P. Wu, H.P. Zhang, S.Y. Guan, R. Holze, *Electrochim. Commun.* 11 (2009) 1325.
- [35] G.J. Wang, Q.T. Qu, B. Wang, Y. Shi, S. Tian, Y.P. Wu, R. Holze, *J. Power Sources* 189 (2009) 503.
- [36] Q.T. Qu, B. Wang, L.C. Yang, Y. Shi, S. Tian, Y.P. Wu, *Electrochim. Commun.* 10 (2008) 1652.